Preliminary Accuracy Assessment of the F-Layer Worst-Case BDS Scintillation Observed by the GNOS Onboard the FY3D Satellite

Guangyuan Tan ⓘ, Guanglin Yang ⓘ, Jingsong Wang, Weihua Bai ⓘ, Yueqiang Sun, Xiuqing Hu ⓘ, Peng Zhang ⓘ, *Senior Member, IEEE*, Qifei Du, Xianyi Wang, Xiangguang Meng, Congliang Liu, and Peng Hu

Abstract—The FY3C/GNOS launched in 2013 can only detect the scintillation of GPS navigation signals, while the FY3D satellite launched in 2017 supports the scintillation observation of BeiDou navigation satellite system (BDS) signals, thus enabling simultaneous detection of GPS and BDS ionospheric scintillation. This work presents a preliminary accuracy evaluation of BDS ionospheric scintillation observed by the global navigation satellite system (GNSS) occultation sounder (GNOS) onboard the FY3D satellite, to support long-term ionospheric scientific applications based on the BDS system. First, the F-layer worst-case (maximum) amplitude scintillation index ($S4^F_{\max}$) of FY3D-BDS, FY3D-GPS, and COSMIC-GPS are, respectively, quality-controlled, and the spatial-temporal matching of $S4^F_{\max}$ between FY3D-BDS and FY3D-GPS/COSMIC-GPS is performed. Then, based on the statistical deviation (std) of the $S4^F_{\max}$ data pairs, the data accuracy of FY3D-BDS $S4^F_{\max}$ relative to FY3D-GPS and COSMIC-GPS is obtained. The results show that the std of the $S4^F_{\max}$ differences in data pairs between FY3D-BDS and FY3D-GPS/COSMIC-GPS is smaller than 0.1, which proves the high precision of BDS ionospheric scintillation detection of FY3D/GNOS. Meanwhile, the std of the $S4^F_{\max}$ differences between FY3D-BDS and FY3D-GPS/COSMIC-GPS at nighttime is higher than that at daytime, and the std in the mid-latitude region is lower than that in the low-latitude and high-latitude regions.

Index Terms—BeiDou navigation satellite system (BDS), constellation observing system for meteorology ionosphere and climate (COSMIC), FY3D/GNSS occultation sounder (GNOS), ionospheric scintillation, S4, validation.

I. INTRODUCTION

THE ionosphere is a part of the upper atmosphere that is ionized at about 60–1000 km. The ionosphere contains a large amount of plasma composed of free electrons and ions, and the instability of the plasma leads to ionospheric irregularities of various scales. The ionospheric irregularities modulate the navigation signals traveling through them randomly, causing rapid fluctuations in the amplitude/phase of the signals, and this phenomenon is known as ionospheric scintillation [1], [2], [3]. Amplitude scintillation index S4 is an important parameter in ionospheric scintillation research, it is defined as normalized root mean square (rms) of signal intensity

$$S4 = \sqrt{\frac{\langle I^2 \rangle - \langle I \rangle^2}{\langle I \rangle^2}} \tag{1}$$

where *I* represents the signal strength, and the brackets represent the average value of the signal strength over a certain period of time. For ionospheric scintillation, this time period is usually 1 s.

Ionospheric scintillation significantly affects global navigation satellite system (GNSS)-related navigation, positioning, and satellite communication applications, and in severe cases, it can lead to the loss of navigation signal lock and communication interruptions [4], [5].

In view of the importance of ionospheric scintillation, the methods of ionospheric scintillation detection include beacons, sounding rockets, incoherent/coherent scattering radars, GNSS scintillation receivers, radio occultation detection, etc., [6], [7], [8], [9]. As a relatively novel technique, radio occultation can work in all weather conditions with the advantages of global coverage, high precision, high vertical resolution, and low cost. In the late 1990s, the MicroLab-1 occultation experiment in GPS/MET program successfully observed ionospheric parameters, which promoted a series of occultation projects, such

Guangyuan Tan, Weihua Bai, Yueqiang Sun, Qifei Du, Xianyi Wang, Xiangguang Meng, Congliang Liu, and Peng Hu are with the National Space Science Center, Chinese Academy of Sciences, Beijing 100190, China, also with the Beijing Key Laboratory of Space Environment Exploration, Beijing 100190, China, and also with the Key Laboratory of Science and Technology on Space Environment Situational Awareness, CAS, Beijing 100190, China (e-mail: tanguangyuan@nssc.ac.cn; baiweihua@nssc.ac.cn; syq@nssc.ac.cn; dqf@nssc.ac.cn; wxy@nssc.ac.cn; xgmeng@nssc.ac.cn; lcl@nssc.ac.cn; hupeng@nssc.ac.cn).

Guanglin Yang and Jingsong Wang are with the Key Laboratory of Space Weather, National Satellite Meteorological Center, China Meteorological Administration, Beijing 100190, China, and also with the Innovation Center for FengYun Meteorological Satellite, Beijing 100190, China (e-mail: yglyang@cma.gov.cn; wangjs@cma.gov.cn).

Xiuqing Hu and Peng Zhang are with the Key Laboratory of Radiometric Calibration and Validation for Environmental Satellites, National Satellite Meteorological Center, China Meteorological Administration, Beijing 100190, China, and also with the Innovation Center for FengYun Meteorological Satellite, Beijing 100190, China (e-mail: huxq@cma.gov.cn; zhangp@cma.gov.cn).

Digital Object Identifier 10.1109/JSTARS.2022.3204892

as Challenging Minisatellite Payload (CHAMP), Gravity Recovery and Climate Experiment (GRACE), etc., [10], [11], [12]. In 2006, the first international six-satellite occultation constellation, Constellation Observing System for Meteorology Ionosphere and Climate (COSMIC), was successfully launched and put into use, enabling the ionospheric occultation sounding to enter the stage of operational application [13]. Its scientific observations are widely used in modeling and forecasting of ionospheric scintillation, as well as other space weather research [14], [15], [16], [17]. Fengyun III(FY3) plans to deploy six satellites (C, D, E, F, G, R) and utilize the GNSS occultation sounder (GNOS) payloads onboard to conduct occultation surveys of the Earth's neutral atmosphere and ionosphere[18]. Specifically, FY3C was launched in September 2013 in a near-polar sun-synchronous orbit at an inclination of 98.8° and an altitude of 836 km. The GNOS payload onboard FY3C consists of three antennas, three RF units, and one occultation data processing unit, and it has achieved the first international occultation detection of global positioning system (GPS) and BeiDou navigation satellite system (BDS). The three antennas include a positioning antenna, a forward occultation antenna for observing atmospheric/ionospheric rising occultation events, and a backward occultation antenna for observing atmospheric/ionospheric descending occultation events [19], [20].

As a high standard in the field of ionospheric occultation sounding, COSMIC has been widely used in ionospheric scientific research for its ionospheric scintillation data. Bai et al. compared and analyzed the accuracy of GPS ionospheric scintillation of FY3C-GPS with that of COSMIC-GPS [21]. The results show that the standard deviation (std) of the differences in the F-layer worst-case (maximum) scintillation index ($S4_{\max}^F$) between them is less than 0.1, indicating the high accuracy of FY3C/GNOS scintillation detection. As an important part of the FY3 constellation program, FY3D was successfully launched in 2017, three years after the deployment of FY3C-GNOS. FY3C and FY3D form a double-satellite occultation observation network that covers the observation periods in the morning and afternoon. Compared with FY3C/GNOS, the GNOS on FY3D increases the number of GPS and BDS occultation channels and optimizes the gain of the antennas to improve the occultation detection quality. Meanwhile, the number of occultation events increases from 680 (500 GPS+180 BDS) to 800 (580 GPS+220 BDS) per day, and the support for BDS scintillation observation is added, thus enabling simultaneous observation of GPS and BDS scintillation [22]. Fig. 1 shows the global distribution of $S4_{\max}^F$ observed by FY3D-BDS. This work aims to provide the first preliminary assessment of the BDS ionospheric scintillation data detected by FY3D/GNOS with that of FY3D-GPS/COSMIC-GPS, thus proving support for the subsequent development of long-term ionospheric scientific applications based on the BDS.

The rest of this article is organized as follows. Section II introduces the ionospheric scintillation observations of FY3D-BDS, FY3D-GPS, and COSMIC-GPS, gives the selection conditions and the spatial-temporal matching principles of $S4_{\max}^F$ index before accuracy evaluation, introduces the accuracy evaluation methods between $S4_{\max}^F$ indexes, and presents a pair of moderate/strong and weak scintillation data pairs after data screening
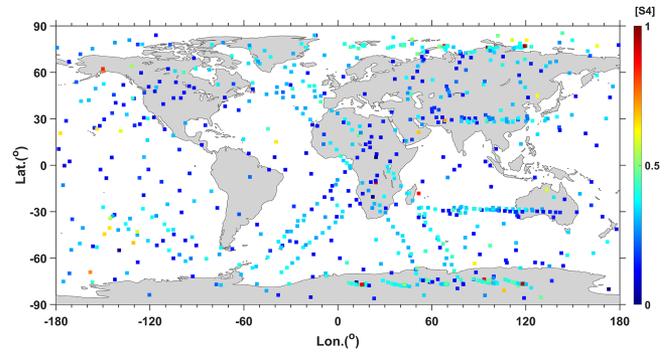

Fig. 1. Global distribution of the worst-case (maximum) F-layer ionospheric scintillation ($S4_{\max}^F$) observed by FY3D/GNOS-BDS from October 1, 2019, to October 7, 2019.
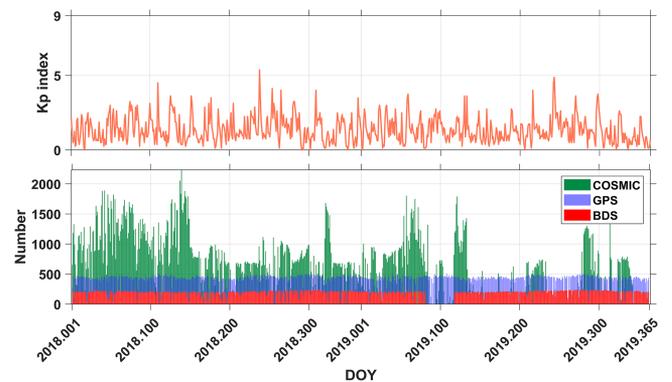

Fig. 2. Variations in the Kp index and the number of FY3D-BDS, FY3D-GPS, and COSMIC-GPS ionospheric occultation events from 2018 to March 23, 2019.

and spatial-temporal matching. In Section III, the comparison results of $S4_{\max}^F$ between FY3D-BDS and FY3D-GPS/COSMIC-GPS are presented. Section IV analyzes the statistical deviation of $S4_{\max}^F$ between FY3D-BDS and FY3D-GPS/COSMIC-GPS, and discusses the related phenomena. Finally, Section V concludes this article.

II. MATERIALS AND METHODOLOGY

A. Scintillation Index Observed by FY3D-BDS, FY3D-GPS, and COSMIC-GPS

The planetary Kp index is derived from three-hourly K indices observed by global specific observatories [23], [24]. It has been extensively used to represent geomagnetic disturbance for scientific and operational purposes on a global scale. Kp index is used by NOAA to describe the geomagnetic storm, ranging from minor (G1) for $Kp = 5$ to extreme (G5) for $Kp = 9$. Also, the index is used to represent scintillations in GNSS signals at high latitudes [25]. As can be seen from the top panel of Fig. 2, there is only one minor geomagnetic storm, and the geomagnetic quiet period dominates in 2018 and 2019. The number of ionospheric occultation events of FY3D-BDS, FY3D-GPS, and COSMIC-GPS from 2018 to 2019 is presented in the bottom panel. It can be seen that the daily occultation events of FY3D-BDS and

FY3D-GPS are around 260 and 480, respectively. After April 2019, only one satellite of the COSMIC-1 constellation works normally, so its scintillation observations decrease sharply. To make the scintillation assessment of FY3D-BDS more statistically significant, this article compares the scintillation data of FY3D-GPS and COSMIC-GPS from 2018.01.01 to 2019.03.23 with FY3D-BDS scintillation data.

The scintillation index (S4) of FY3D/GNOS is calculated from the signal power of GNSS satellites received by GNOS, i.e., the product of the signal transmission power of GNSS satellites and a series of attenuation coefficients. The specific calculation formula is as follows, more details can be found in Weihua Bai et al. [21]

$$S4_i = \sqrt{\frac{\langle P_i^2 \rangle_T - \langle P_i \rangle_T^2}{\langle P_i \rangle_T^2}} \qquad (2)$$

where i denotes the ith GNSS satellite, P denotes the power of the GNSS signal received by GNOS, the $\langle . \rangle_T$ represent the average value of the parameters inside brackets during period T. The $\langle P_i \rangle_T$ and $\langle P_1^2 \rangle_T$ sampled at 50 Hz in 1 s is downlinked from the FY3D/GNOS to the ground processing center for S4 calculation.

B. Selection Condition of Ionospheric Scintillation Index

Straus [26] and Dymond [7] approximated the position of the radio occultation scintillation at the tangent point of the occultation ray and compared it with other observations. The results indicate that the scintillation morphology between them is in good agreement. Thus, the above approximation method is used in this work. In the ascending/descending ionospheric occultation events, the scintillation in the E layer may come from the F layer [21]. To prevent the interference from other regions, the scintillation in the F-layer (200–450 km) is selected, and its worst-case (maximum) amplitude scintillation index ($S4_{max}^F$) during the occultation event is used as the evaluation parameter of the FY3D-BDS scintillation. Meanwhile, to ensure the integrity and detection quality of the $S4_{max}^F$ parameter, the signal-to-noise ratio (SNR) during the occurrence of $S4_{max}^F$ is constrained. The specific conditions are as follows:

1) $S4_{max}^F$ must occur within the F-layer (200–450km) of the ionosphere.
2) The SNR of the signal 10 s before and after $S4_{max}^F$ detection cannot be 0.
3) In the occultation event where $S4_{max}^F$ is located, the data loss cannot occur within 200–450 km.

The statistical distribution of $S4_{max}^F$ of FY3D-BDS, FY3D-GPS, and COSMIC-GPS is shown in the Fig. 3. Since the period from 2018.01.01 to 2019.03.23 is in the quiet period of solar activity, as can be seen in the upper panel of Fig. 2, more than 96% of the scintillation indices were lower than 0.25, that is, no scintillation (0∼0.08) or low/weak scintillation (0.09∼0.25), the moderate (0.26∼0.5) and strong (>0.5) accounts for less than 4% in the whole period [27], [28], as can be seen in the enlarged part in Fig. 3.
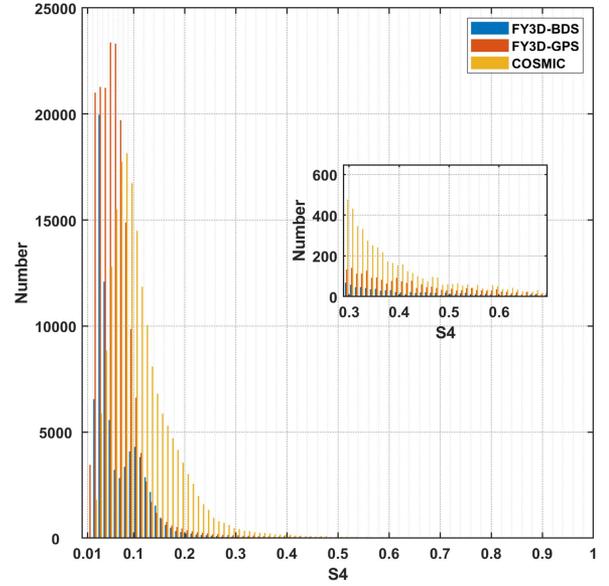

Fig. 3.   Statistical distributions of $S4_{max}^F$ for FY3D-BDS (blue bar), FY3D-GPS (red bar), and COSMIC-GPS (orange bar). The parts with $S4_{max}^F > 0.3$ are enlarged and annotated in the figure.

C. Matching Principles of $S4_{max}^F$ Between FY3D-BDS and FY3D-GPS/COSMIC-GPS

Before the $S4_{max}^F$ of FY3D-BDS is compared with that of FY3D-GPS and COSMIC-GPS to obtain the $S4_{max}^F$ error characteristics, the $S4_{max}^F$ between them needs to be matched into data pairs in time and space. If the temporal and spatial matching conditions are too loose, the two $S4_{max}^F$ parameters are not meaningful for the comparison; if the conditions are too strict, there are too few matched pairs, and the comparison results will lose statistical significance. To address this issue, this article considers the spatial-temporal matching degree of the $S4_{max}^F$ data and the number of valid data matching pairs, and makes full reference to the spatial-temporal constraints in previous works on ionospheric product evaluation [21], [29], [30], [31]. In this article, the two $S4_{max}^F$ indexes meet the following principles at the same time, and they can be matched into data pairs for subsequent accuracy assessment. Some specific examples of $S4_{max}^F$ data pairs will be given in Section II-E.

1) The difference in observation time between the two $S4_{max}^F$ parameters are within 2.5 h.
2) The difference between latitude/longitude of the two $S4_{max}^F$ parameters are within 2°.
3) The difference between azimuth angles of the two $S4_{max}^F$ parameters are within 30°.

D. Accuracy Evaluation for FY3D-BDS Scintillation

To evaluate the accuracy of FY3D-BDS amplitude scintillation relative to FY3D-GPS/COSMIC-GPS, the std of $S4_{max}^F$ differences in data pairs is calculated according to the following equation:

$$Ab\_err = S4_{BDS\,max}^F - S4_{TBD\,max}^F \qquad (3)$$

$$\sigma(\text{err}) = \sqrt{\frac{\sum\limits_{i=1}^{N}\left(Ab\_\text{err}_i - E(Ab\_\text{err})\right)^2}{N}}. \qquad (4)$$

In (3), $S4^F_{\text{BDSmax}}$ represents the $S4^F_{\text{max}}$ observed by FY3D-BDS, $S4^F_{\text{TBDmax}}$ represents the $S4^F_{\text{max}}$ of FY3D-GPS or COSMIC-GPS, and Ab_err represents the absolute difference between two $S4^F_{\text{max}}$ parameters in data pair. The std of the $S4^F_{\text{max}}$ differences in the data pairs are calculated according to (4) to obtain the accuracy of FY3D-BDS scintillations, i.e., the deviation of FY3D-BDS scintillations relative to FY3D-GPS/COSMIC-GPS.

E. Examples of $S4_{max}$ Matched Data Pairs

After performing spatial-temporal matching of $S4^F_{\text{max}}$ between FY3D-BDS and FY3D-GPS, there are 21 moderate ($S4>0.26$) and 4 strong ($S4>0.5$) $S4^F_{\text{max}}$ data pairs. And there is 1 moderate $S4^F_{\text{max}}$ data pair between FY3D-BDS and COSMIC-GPS. Thus, we present one strong $S4^F_{\text{max}}$ data pair between FY3D-BDS and FY3D-GPS in Fig. 4, and one moderate $S4^F_{\text{max}}$ data pair between FY3D-BDS and COSMIC-GPS in Fig. 5. Then, we present two weak $S4^F_{\text{max}}$ data pairs between FY3D-BDS and FY3D-GPS/COSMIC-GPS in Figs. 6 and 7.

In Fig. 4, the upper panel [Fig. 4(a)] represents the geometry of the occultation rays between GNSS satellites and LEO satellites when the spatial-temporally matched $S4^F_{\text{max}}$ is detected; the bottom panel [Fig. 4(b)] represents the variation of the S4 index, the latitude and longitude of the occultation tangent point, the azimuth angle of the occultation ray, and the SNR of the occultation signal with the altitude of the occultation tangent point, in the ionospheric occultation events to which the above two $S4^F_{\text{max}}$ belong. It can be seen from the top panel that the $S4^F_{\text{max}}$ of FY3D-BDS, FY3D-GPS are, respectively, 0.53 and 0.55, indicating a strong scintillation level; the altitude of the occultation ray tangent points of $S4^F_{\text{max}}$ detection are, respectively, 257.8 and 247.2 km, which are located in the height range of 200–450 km, i.e., the F layer in the ionosphere. Meanwhile, it can be seen from the Fig. 4(b) that within 10s before and after the detection of $S4^F_{max}$, the SNR of FY3D-BDS, FY3D-GPS are all higher than 0 and are stable at around 500 and 700, respectively. In addition, the longitude and latitude of the occultation tangent point, the azimuth angle of the occultation ray, the amplitude scintillation index, and the SNR remain continuous in the corresponding occultation events, thus proving the effectiveness of scintillation data selection in Section II-B.

The azimuth angles of the occultation rays at $S4^F_{\text{max}}$ observed by FY3D-BDS, FY3D-GPS are, respectively, 136.7° and 136.8°, and they are close to each other; the latitudes of the occultation tangent points at $S4^F_{\text{max}}$ are, respectively, 2.6° and 1.1°, the deviations of latitudes between FY3D-BDS and FY3D-GPS are less than 2°. The longitudes of the occultation tangent points at the time of $S4^F_{\text{max}}$ detection is, respectively, $-179.2°$ and $-177.6°$, and the deviations between them are also less than 2°; the UTC (Universal Time Coordinated) at $S4^F_{\text{max}}$ detection are almost the same. The presentation of the $S4^F_{\text{max}}$ data matching pair of FY3D-BDS with FY3D-GPS shows the effectiveness of
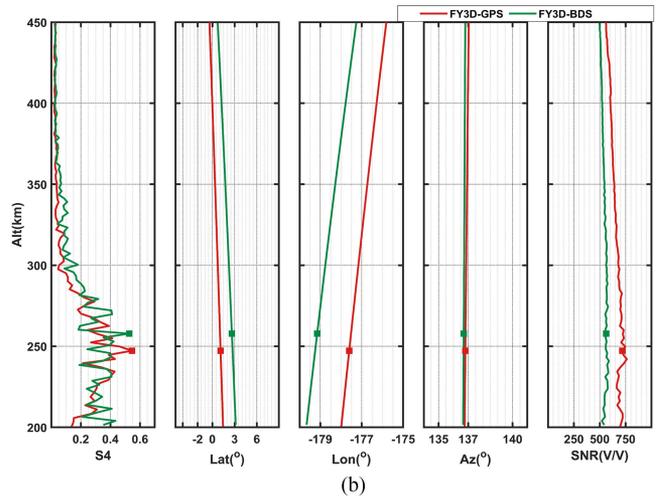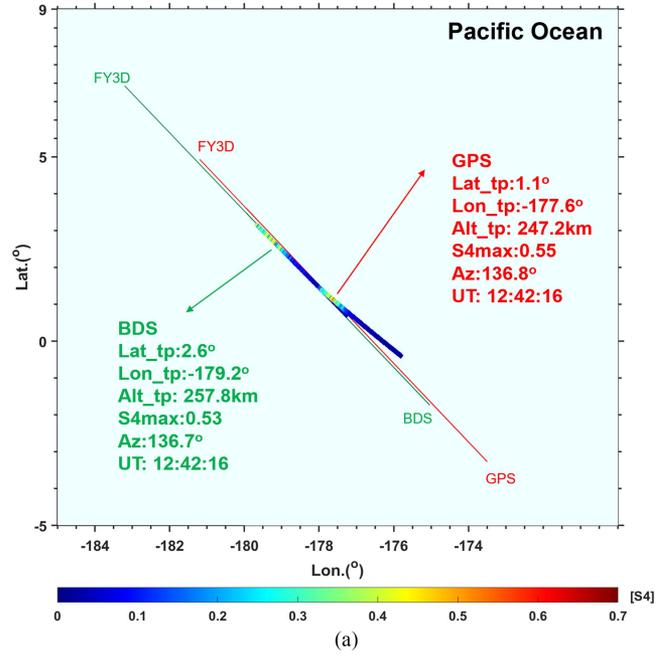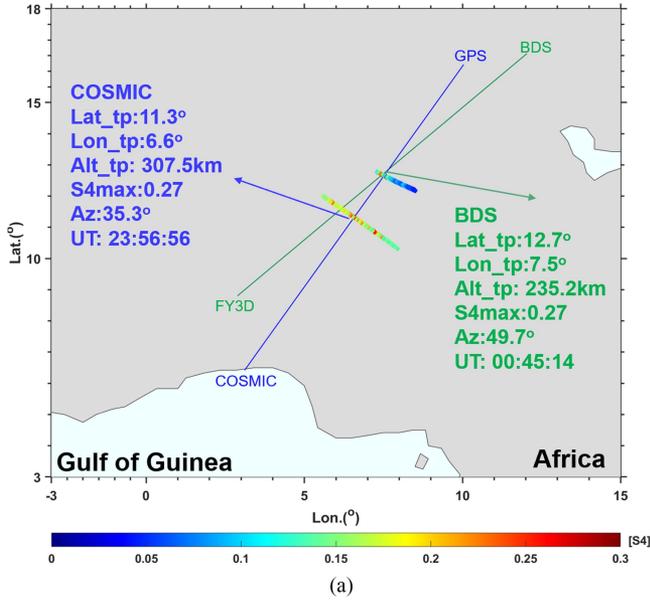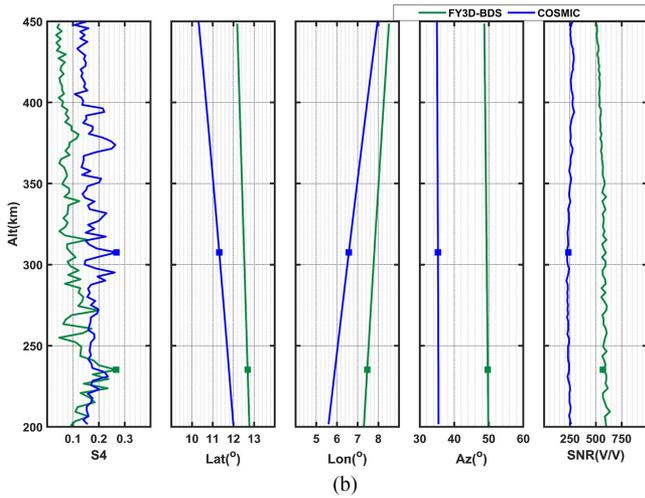

(a)

(b)

Fig. 4. Strong $S4^F_{\text{max}}$ scintillation index for FY3D-BDS vs. FY3D-GPS on April 17, 2018. Fig. 4(a) shows the occultation ray geometry of FY3D-BDS and FY3D-GPS when $S4^F_{\text{max}}$ is detected (represented as green and red lines). The color block represents the detected S4 index, and the intersection of the color block and the occultation ray is the position of the detected $S4^F_{\text{max}}$. When $S4^F_{\text{max}}$ is detected, the latitude, longitude, and height of the occultation ray tangent point, the azimuth angle of the occultation ray, the value of $S4^F_{\text{max}}$ and the UTC time are all marked in the figure. Fig. 4(b) shows the changes of the S4 index, the latitude and longitude of the occultation tangent point, the azimuth angle of the occultation ray, and the SNR of the signal with the altitude in the F-layer. The above ionospheric parameters corresponding to the detection of $S4^F_{\text{max}}$ are marked with squares in the figure.

the spatial-temporal matching principles of the $S4^F_{\text{max}}$ index in Section II-C.

Fig. 5 presents the moderate $S4^F_{\text{max}}$ data pair between FY3D-BDS and COSMIC-GPS. Fig. 5(a) shows that the $S4^F_{\text{max}}$ of FY3D-BDS, COSMIC-GPS are, respectively, 0.27 and 0.27, indicating a moderate scintillation level; the altitude of the occultation ray tangent points are, respectively, 235.2 and 307.5 km,
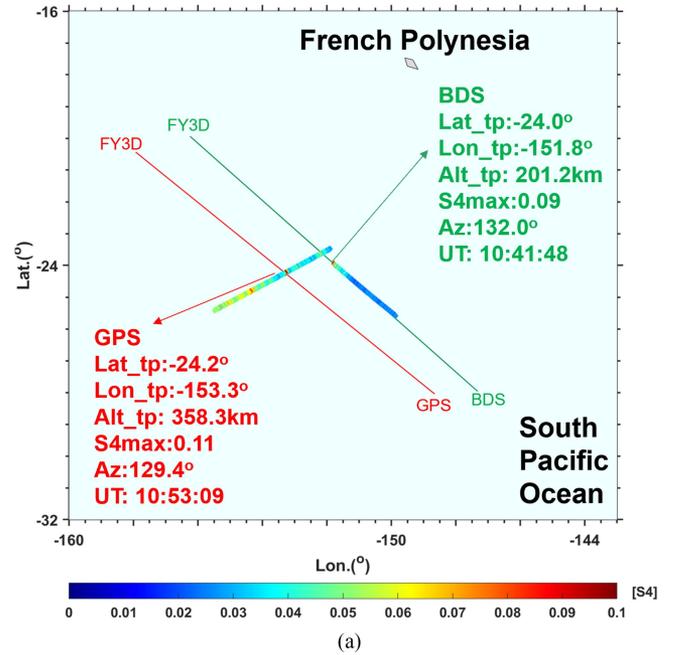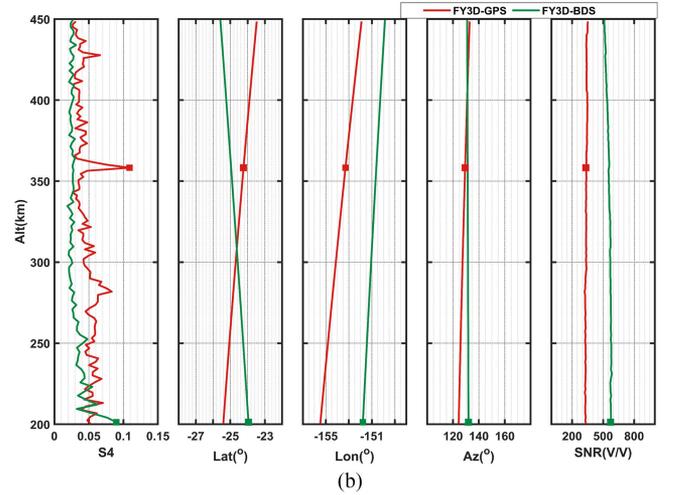
Fig. 5. Moderate $S4_{max}^F$ scintillation index for FY3D-BDS versus COSMIC-GPS on September 7, 2018. Fig. 5(a) shows the occultation ray geometry of FY3D-BDS, COSMIC-GPS when $S4_{max}^F$ is detected (represented as green, blue lines). More details can be seen in Fig. 4.

Fig. 6. Weak $S4_{max}^F$ scintillation index for FY3D-BDS versus FY3D-GPS on March 7, 2018. Fig. 6(a) shows the occultation ray geometry of FY3D-BDS and FY3D-GPS when $S4_{max}^F$ is detected (represented as green, red lines). The detailed explanations can be found in Fig. 4.

which are located in the F layer in the ionosphere. Meanwhile, Fig. 5(b) shows that within 10 s before and after the detection of $S4_{max}^F$, the SNR of FY3D-BDS and COSMIC-GPS are all higher than 0 and are stable at around 600 and 250, respectively. In addition, the parameters in Fig. 5(b) remain continuous in the corresponding occultation events, thus proving the effectiveness of scintillation data selection.

The azimuth angles of the occultation rays at $S4_{max}^F$ observed by FY3D-BDS and COSMIC-GPS are, respectively, 49.7° and 35.3°, with a difference within 30°; the latitudes of the $S4_{max}^F$ tangent points are, respectively, 12.7° and 11.3°, with a deviation less than 2°. The longitudes of the tangent points at $S4_{max}^F$ detection is, respectively, 7.5° and 6.6°, with a deviation less than 2°, either; the UTC deviation at $S4_{max}^F$ detection are less than 2.5 h, either. The $S4_{max}^F$ data matching pair of FY3D-BDS with

COSMIC-GPS shows the effectiveness of the spatial-temporal matching principles like the strong scintillation pair above.

In the weak scintillation event shown in Figs. 6 and 7, it can be seen from the bottom panels that, the $S4_{max}^F$ data pairs of FY3D-BDS versus FY3D-GPS and FY3D-BDS versus. COSMIC-GPS are all within the ionospheric F-layer range, the SNRs of the occultation rays are valid for 10 s before and after the $S4_{max}^F$ detection, and there is no data loss in the ionospheric occultation event, so the $S4_{max}^F$ matching pair in occultation events satisfy the data selection condition in Section II-B. The top panels show that the latitude and longitude of the occultation tangent point, the azimuth angle of the occultation ray, and the observation time of $S4_{max}^F$ are all within the thresholds set in Section II.C. Therefore, the current weak $S4_{max}^F$ data pair
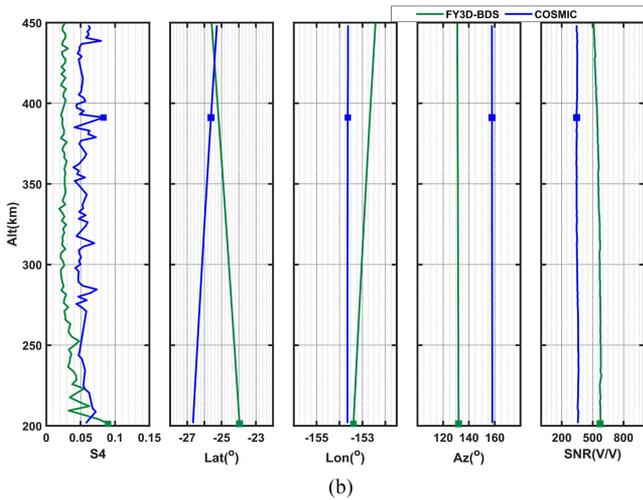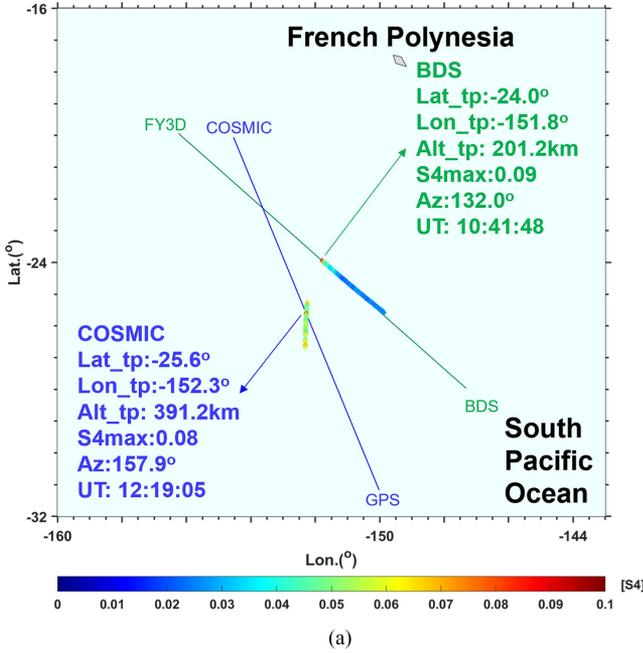
(a)

(b)

Fig. 7. Weak $S4_{\max}^{F}$ scintillation index for FY3D-BDS versus COSMIC-GPS on March 7, 2018. The top panel shows the occultation ray geometry of FY3D-BDS, COSMIC-GPS at $S4_{\max}^{F}$ (represented as green, blue lines). The detailed explanations can be found in Fig. 4.

between FY3D-BDS and FY3D-GPS/COSMIC-GPS also meet the spatial-temporal matching principles.

III. RESULTS

A. $S4_{max}^{F}$ Validation Between FY3D-BDS and FY3D-GPS

This section presents the global distribution of $S4_{\max}^{F}$ matching pairs between FY3D-BDS and FY3D-GPS in Fig. 8, the global differences of $S4_{\max}^{F}$ pairs in Fig. 9, and $S4_{\max}^{F}$ statistical deviations in Fig. 10.

It can be seen from Fig. 8 that the $S4_{\max}^{F}$ data of FY3D-BDS and FY3D-GPS can still achieve a global distribution even after the data matching. Since FY3D receives navigation signals from
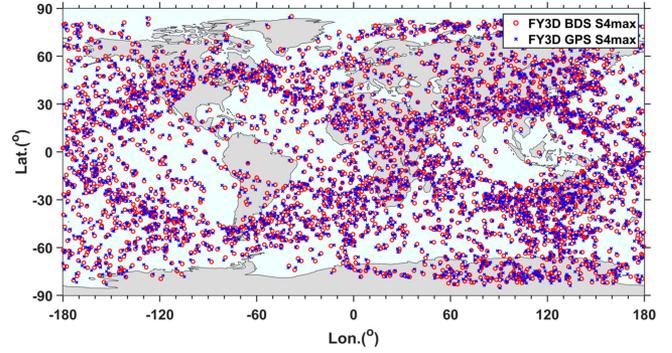

Fig. 8. Global distribution of the spatial-temporal matched $S4_{\max}^{F}$ data pairs between FY3D-BDS and FY3D-GPS from January 1, 2018 to March 23, 2019.
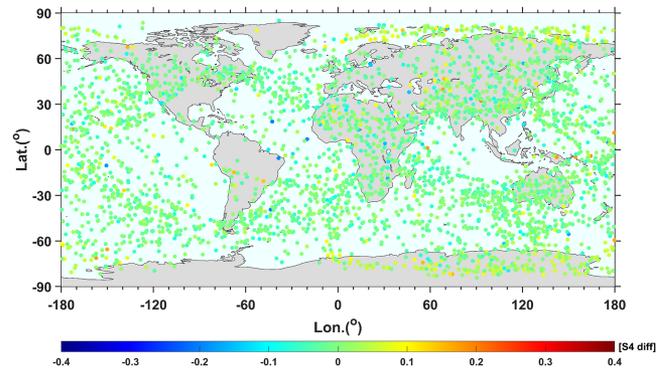

Fig. 9. Global distribution of the deviations of $S4_{\max}^{F}$ data pairs between FY3D-BDS and FY3D-GPS from January 1, 2018 to March 23, 2019.

the regional BDS-2 constellation, the $S4_{\max}^{F}$ data pairs are more densely distributed in the Asian sector. From Fig. 9, it can be seen that the absolute deviation of most $S4_{\max}^{F}$ data pairs is around 0. Also, the color blocks are mostly in light green ($\sim$0), qualitatively showing the small systematic deviation of $S4_{\max}^{F}$ between FY3D-BDS and FY3D-GPS.

To comprehensively evaluate statistical deviations of $S4_{\max}^{F}$ data pairs between FY3D-BDS and FY3D-GPS, this article divides the $S4_{\max}^{F}$ matching pairs into daytime (0600$\sim$1800 LT), nighttime (1800 $\sim$0600 LT), low latitude (-30°$\sim$30°), mid-latitude (-30°$\sim$-60°, 30°$\sim$60°), and high latitude (-60°$\sim$-90°, 60°$\sim$90°) to assess the bias and std of $S4_{\max}^{F}$ data pairs, respectively. It can be seen from Fig. 10 that the $S4_{\max}^{F}$ differences between FY3D-BDS and FY3D-GPS belong to a quasi-normal distribution with a mean value of about 0, and most $S4_{\max}^{F}$ differences are concentrated in the range of -0.05 to 0.05. During the whole day, the bias and std of $S4_{\max}^{F}$ differences are, respectively, -0.0065 and 0.0419; during the daytime, the bias and std are, respectively, -0.0049 and 0.0418; during nighttime, the bias and std are, respectively, -0.0080 and 0.0420. In addition, in the low latitude, the bias and std are, respectively, -0.0122 and 0.0420; in the middle latitude, bias and std are, respectively, -0.0121 and 0.0355; in the high latitude, the bias and std are, respectively, 0.0169 and 0.0462. Thus, when divided by the local time, the std of $S4_{\max}^{F}$ differences during the nighttime is higher than that
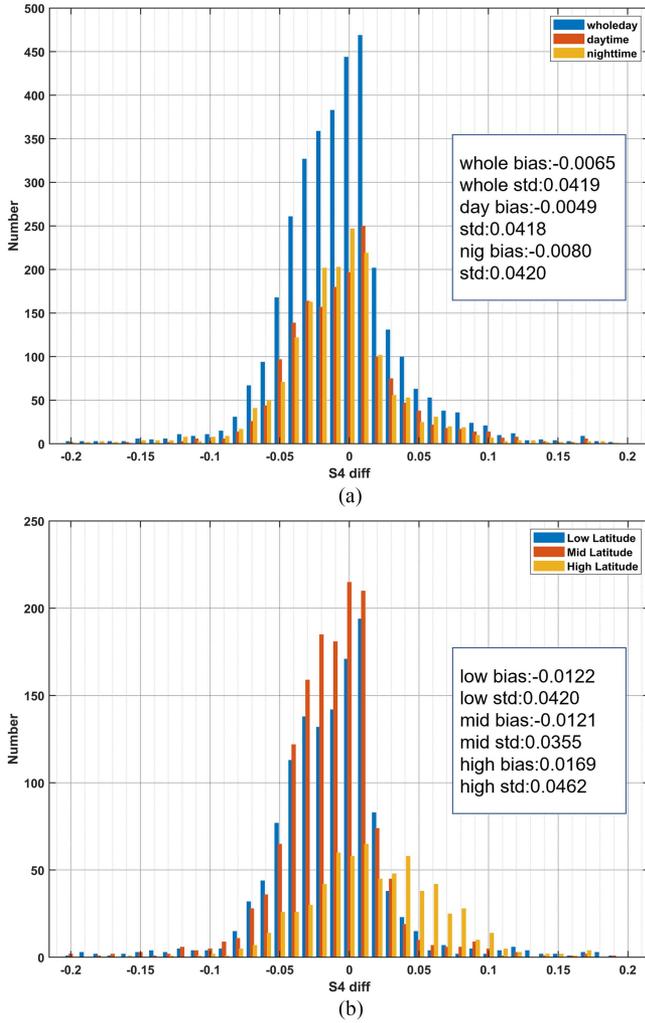
(a)

(b)

Fig. 10.   Statistical distribution of the bias and std of $S4_{max}^F$ data pair difference between FY3D-BDS and FY3D-GPS from January 1, 2018 to March 23, 2019, in the whole day, daytime, nighttime, low latitude, mid-latitude, and high latitude. In the top panel, the blue, red, and orange bars indicate the deviations of $S4_{max}^F$ data pairs in the whole day, day, and night, respectively; in the bottom panel, the three bars describe the differences of $S4_{max}^F$ data pairs in the low, middle, and high latitudes, respectively.

during the daytime; when divided by latitude, the std of the middle latitude is the smallest, and the std of the low latitude and high latitude is larger.

B. $S4_{max}^F$ Validation Between FY3D-BDS and COSMIC-GPS

This part presents the global distribution and statistical deviation of the $S4_{max}^F$ matching pairs between FY3D-BDS and COSMIC-GPS. Fig. 11 shows the global distribution of $S4_{max}^F$ matching pairs between FY3D-BDS and COSMIC-GPS; Fig. 12 shows the global deviation of $S4_{max}^F$ matching pairs; Fig. 13 shows the statistical deviation of global $S4_{max}^F$ matching pairs. To evaluate the statistical deviation of the $S4_{max}^F$ pairs between FY3D-BDS and COSMIC-GPS more comprehensively, the $S4_{max}^F$ pairs are divided into daytime, nighttime, low latitude,
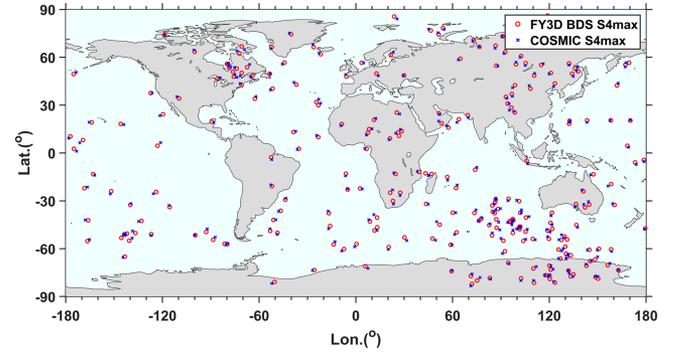

Fig. 11.   Global distribution of the spatial-temporal matched $S4_{max}^F$ data pairs between FY3D-BDS and COSMIC-GPS from January 1, 2018 to March 23, 2019.
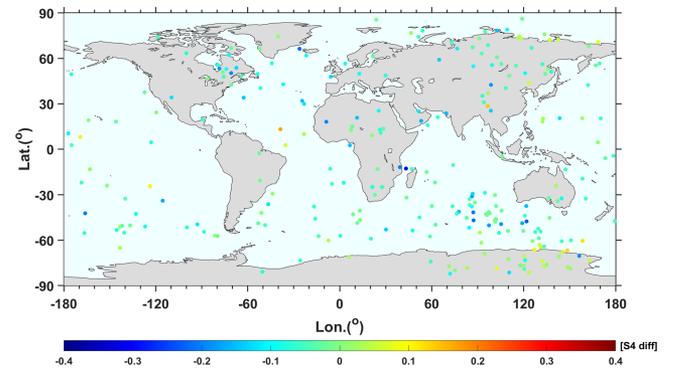

Fig. 12.   Global distribution of the deviations of $S4_{max}^F$ data pairs between FY3D-BDS and COSMIC-GPS from January 1, 2018 to March 23, 2019.

middle latitude, and high latitude to assess the corresponding bias and std, in Fig. 13.

It can be seen from Fig. 11 that as the number of valid COSMIC payloads decreases, the number of $S4_{max}^F$ data pairs between FY3D-BDS and COSMIC-GPS is smaller than that between FY3D-BDS and FY3D-GPS, but there is a uniform distribution of $S4_{max}^F$ pairs in all sectors of the world. In Fig. 12, the absolute deviation of most $S4_{max}^F$ matching pairs is about 0, i.e., most of the color patches are in light green (∼0), which qualitatively shows a small systematic offset of $S4_{max}^F$ between FY3D-BDS and COSMIC-GPS. Fig. 13 quantitatively presents the statistical deviation of $S4_{max}^F$ between FY3D-BDS and COSMIC-GPS, i.e., the scintillation accuracy of FY3D-BDS relative to COSMIC-GPS. It can be seen from the top and bottom panels that the $S4_{max}^F$ differences conform to a basic quasi-normal distribution but with a systematic offset of around -0.05, indicating that the scintillation index observed by FY3D-BDS is slightly lower than that of COSMIC-GPS. In the top panel, there are 259 pairs of $S4_{max}^F$ in the whole day, and the systematic deviation between FY3D-BDS and COSMIC is -0.0445, with a std of 0.0702. In the daytime, the bias between FY3D-BDS and COSMIC-GPS is -0.0477, with a std of 0.0622, and in the nighttime, the bias is -0.0411, with a std of 0.0779. Besides, the bias and std between FY3D-BDS and
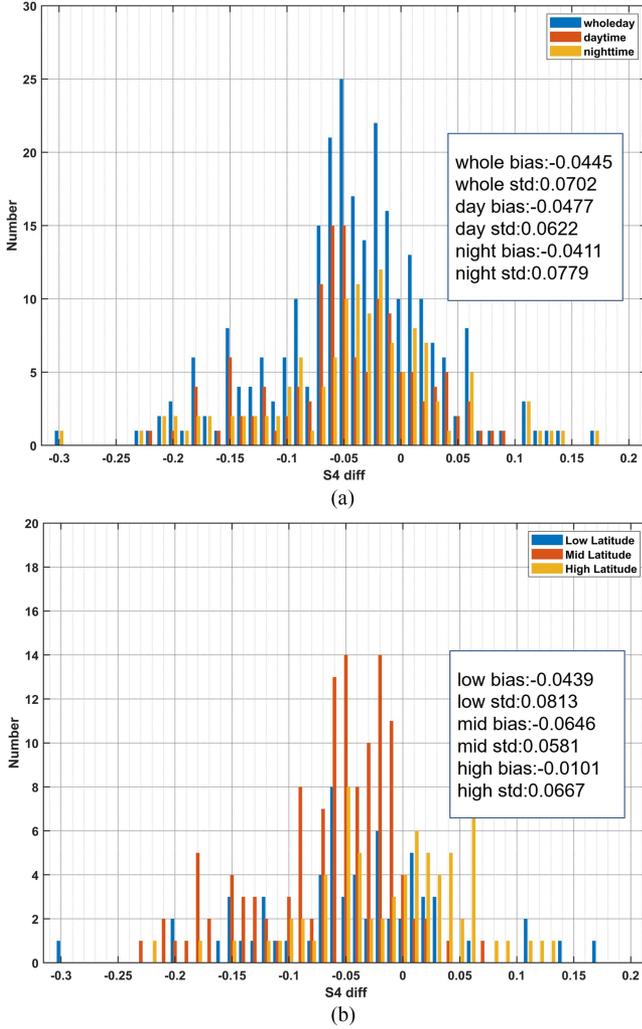
Fig. 13. Statistical distribution of bias and std of the $S4^F_{\max}$ data pair difference between FY3D-BDS and COSMIC-GPS from January 1, 2018 to March 23, 2019, in the whole day, daytime, nighttime, low latitude, mid-latitude, and high latitude.

TABLE I
STATISTICAL DEVIATIONS OF $S4^F_{\mathrm{MAX}}$ BETWEEN FY3D-BDS AND FY3D-GPS FROM 2018.01.01 TO 2019.03.23

Period	FY3D-BDS Mean	FY3D-GPS Mean	Bias	Std	Number
Whole day	0.0607	0.0671	-0.0065	0.0419	3401
Daytime	0.0569	0.0618	-0.0049	0.0418	1671
Nighttime	0.0643	0.0723	-0.0080	0.0420	1730
Low Latitude	0.0605	0.0727	-0.0122	0.0420	1300
Mid Latitude	0.0473	0.0594	-0.0121	0.0355	1437
High Latitude	0.0899	0.0730	0.0169	0.0462	664

TABLE II
STATISTICAL DEVIATIONS OF $S4^F_{\mathrm{MAX}}$ BETWEEN FY3D-BDS AND COSMIC-GPS FROM 2018.01.01 TO 2019.03.23

Period	FY3D-BDS Mean	COSMIC Mean	Bias	Std	Number
Whole day	0.0625	0.1069	-0.0445	0.0702	259
Daytime	0.0565	0.1042	-0.0477	0.0622	132
Nighttime	0.0686	0.1097	-0.0411	0.0779	127
Low Latitude	0.0641	0.1080	-0.0439	0.0813	62
Mid Latitude	0.0459	0.1105	-0.0646	0.0581	125
High Latitude	0.0898	0.0998	-0.0101	0.0667	72

the deviations of the $S4^F_{\max}$ pairs between FY3D-BDS and FY3D-GPS basically conform to a quasi-normal distribution, the number of data pairs with negative deviations is more than that with positive deviations, which is consistent with results in Table I. In Table II, the average $S4^F_{\max}$ of FY3D-BDS is still lower than that of COSMIC in whole day, but the magnitude increases to about 0.04. In Fig. 13, the $S4^F_{\max}$ differences between FY3D-BDS and COSMIC-GPS also show an obvious mean-negative quasi-normal-like distribution. The systematic bias between FY3D-BDS and FY3D-GPS may be caused by the signal strengths of different navigation signals. And the systematic offset between FY3D-BDS and COSMIC-GPS is also affected by the thermal noise of different detection payload and the S4 calculation method, except the above factor. Since FY3D S4 is calculated based on the signal strength as described in Section II-A, the COSMIC S4 is calculated from the one-second average SNR and the rms of the signal strength [32]. The explanation of the larger systematic offset of $S4^F_{\max}$ between FY3D-BDS and COSMIC-GPS will be described in the next paragraph.

Taking std as the $S4^F_{\max}$ accuracy evaluation standard, at the whole day, the $S4^F_{\max}$ std between FY3D-BDS and FY3D-GPS is 0.0419, and the $S4^F_{\max}$ std between FY3D-BDS and COSMIC is 0.0702. The latter is larger than the former, and this is mainly caused by two factors. One factor is that the COSMIC constellation has reached the end of its life cycle in 2018–2019, and the number of valid payloads declined sharply. Therefore, compared with FY3D-GPS versus FY3D-BDS, there are fewer $S4^F_{\max}$ data matching pairs between FY3D-BDS and COSMIC-GPS, so the $S4^F_{\max}$ std may increase statistically. The other factor is that the $S4^F_{\max}$ of FY3D-BDS and FY3D-GPS is retrieved from different GNSS signals received by the same GNOS payload, while the $S4^F_{\max}$ of FY3D-BDS and COSMIC-GPS is generated from different GNSS signals received by different payloads. The former

COSMIC-GPS are -0.0439 and 0.0813 in low latitude, -0.0646 and 0.0581 in middle latitude, and -0.0101 and 0.0667 in high latitude. The variation of $S4^F_{\max}$ error characteristics between FY3D-BDS and COSMIC-GPS in the local time and latitude is similar to that between FY3D-BDS and FY3D-GPS. The $S4^F_{\max}$ std in the nighttime is higher than that in the daytime, while the std in the middle latitude is the lowest.

IV. DISCUSSION

Tables I and II show the statistical deviation of the $S4^F_{\max}$ data between FY3D-BDS and FY3D-GPS/COSMIC-GPS in the whole day, daytime, nighttime, low latitudes, middle latitudes, and high latitudes from January 1, 2018 and to March 23, 2019. It can be seen from Table I that the average $S4^F_{\max}$ of FY3D-BDS is slightly lower than that of FY3D-GPS, except in the high latitudes where the number of $S4^F_{\max}$ data matching pairs is smaller. Meanwhile, it can be seen from Fig. 10 that, although

is the internal coincidence accuracy comparison of $S4_{\max}^F$, while the latter is the external coincidence accuracy comparison, so the $S4_{\max}^F$ deviation of the former may be lower than that of the latter. Overall, the std of $S4_{\max}^F$ differences between FY3D-BDS and FY3D-GPS/COSMIC-GPS is lower than 0.1, indicating the high precision of FY3D-BDS scintillation detection.

In addition, the $S4_{\max}^F$ std between FY3D-BDS and FY3D-GPS/COSMIC-GPS at nighttime is higher than that at daytime. This is due to the change of ionospheric irregularities postmidnight[33] and the disparity of spatial-temporal matching principles. After midnight, the plasma bubbles will intensify sharply in the ionosphere. Although spatial-temporal constraints are put on the occurrence conditions of the worst-case scintillation in the F-layer, when each GNSS signal passes through the irregularities at different azimuth angles, times, and geographical positions, the amplitude/phase of the GNSS signal will be modulated differently, thus increasing the $S4_{\max}^F$ deviation in the data pairs at nighttime.

It can also be observed that the $S4_{\max}^F$ between FY3D-BDS and FY3D-GPS/COSMIC-GPS is closest in the middle latitude, i.e., the std between them is the smallest, while the std in the high latitude and low latitude areas is larger. The study conducted by Tsai et al. shows that during the quiet period of solar activity, ionospheric irregularities occur more frequently at low latitudes and high latitudes but less frequently at middle latitudes [28]. Thus, low latitude and high latitude will have a higher probability of generating ionospheric irregularities, thus increasing the random variation of $S4_{\max}^F$ and leading to the corresponding enhancement of $S4_{\max}^F$ std.

The GNOS payload onboard FY3D can only receive GNSS signals of the regional BDS-2 system, while the GNOS-II onboard the FY3E satellite can receive signals of the global BDS-3 system. Thus, it is urgent to evaluate the accuracy of the ionospheric scintillation of BDS-3 received by the GNOS-II payload onboard FY3E satellite. Since COSMIC-2 has accumulated a large amount of ionospheric scintillation data, our future work will match the scintillation index of FY3E-BDS with COSMIC-2 in time and space for accuracy evaluation and compare their global ionospheric scintillation morphology.

V. CONCLUSION

This article presents the global distribution and the statistical deviation of the spatial-temporal matched $S4_{\max}^F$ data pairs between FY3D-BDS and FY3D-GPS/COSMIC-GPS from January 1, 2018 to March 23, 2019. The results indicate that the $S4_{\max}^F$ observed by FY3D-BDS is slightly lower than that of FY3D-GPS and COSMIC-GPS. Also, the std of $S4_{\max}^F$ differences between FY3D-BDS and FY3D-GPS/COSMIC-GPS is smaller than 0.1, showing the high precision of the scintillation observation of FY3D-BDS, which provides a scientific reference for the subsequent research and application of the S4 index from FY3D-BDS in ionospheric study.

ACKNOWLEDGMENT

REFERENCES

[1] A. W. Wernik, J. A. Secan, and E. J. Fremouw, "Ionospheric irregularities and scintillation," *Adv. Space Res.,* vol. 31, no. 4, pp. 971–981, 2003.

[2] X. Pi, A. J. Mannucci, U. J. Lindqwister, and C. M. Ho, "Monitoring of global ionospheric irregularities using the worldwide GPS network," *Geophys. Res. Lett.,* vol. 24, no. 18, pp. 2283–2286, 1997.

[3] B. G. Fejer and M. C. Kelley, "Ionospheric irregularities," *Rev. Geophys.,* vol. 18, no. 2, pp. 401–454, 1980.

[4] L. A. Salles, B. C. Vani, A. Moraes, E. Costa, and E. R. de Paula, "Investigating ionospheric scintillation effects on multifrequency GPS signals," *Surv. Geophys.,* vol. 42, no. 4, pp. 999–1025, 2021.

[5] R. S. Conker, M. B. El-Arini, C. J. Hegarty, and T. Hsiao, "Modeling the effects of ionospheric scintillation on GPS/satellite-based augmentation system availability," *Radio Sci.,* vol. 38, no. 1, pp. 1-1–1-23, 2003.

[6] M. C. Kelley, K. D. Baker, J. C. Ulwick, C. L. Rino, and M. J. Baron, "Simultaneous rocket probe, scintillation, and incoherent scatter radar observations of irregularities in the auroral zone ionosphere," *Radio Sci.,* vol. 15, no. 3, pp. 491–505, 1980.

[7] K. F. Dymond, "Global observations of l band scintillation at solar minimum made by COSMIC," *Radio Sci.,* vol. 47, no. 04, pp. 1–10, 2012.

[8] Y. Béniguel et al., "Ionospheric scintillation monitoring and modelling," *Ann. Geophys.,* vol. 52, no. 3/4, pp. 391–416, 2009.

[9] T. L. Beach and P. M. Kintner, "Development and use of a GPS ionospheric scintillation monitor," *IEEE Trans. Geosci. Remote Sens.,* vol. 39, no. 5, pp. 918–928, May 2001.

[10] W. S. Schreiner, S. V. Sokolovskiy, C. Rocken, and D. C. Hunt, "Analysis and validation of GPS/MET radio occultation data in the ionosphere," *Radio Sci.,* vol. 34, no. 4, pp. 949–966, 1999.

[11] M. E. Gorbunov and L. Kornblueh, "Analysis and validation of GPS/MET radio occultation data," *J. Geophys. Res.,* vol. 106, no. D15, pp. 17161–17169, 2001.

[12] J. Wickert et al., "GPS radio occultation with CHAMP and GRACE: A first look at a new and promising satellite configuration for global atmospheric sounding," *Ann. Geophys.,* vol. 23, no. 3, pp. 653–658, 2005.

[13] Y.-A. Liou et al., "FORMOSAT-3/COSMIC GPS radio occultation mission: Preliminary results," *IEEE Trans. Geosci. Remote Sens.,* vol. 45, no. 11, pp. 3813–3826, Nov. 2007.

[14] S.-P. Chen, D. Bilitza, J.-Y. Liu, R. Caton, L. C. Chang, and W.-H. Yeh, "An empirical model of L-band scintillation S4 index constructed by using FORMOSAT-3/COSMIC data," *Adv. Space Res.,* vol. 60, no. 5, pp. 1015–1028, 2017.

[15] R. A. Anthes, "Exploring Earth's atmosphere with radio occultation: Contributions to weather, climate and space weather," *Atmos. Meas. Tech.,* vol. 4, no. 6, pp. 1077–1103, 2011.

[16] J. Y. Liu, S. P. Chen, W. H. Yeh, H. F. Tsai, and P. K. Rajesh, "Worst-case GPS scintillations on the ground estimated from radio occultation observations of FORMOSAT-3/COSMIC during 2007–2014," *Surv. Geophys.,* vol. 37, no. 4, pp. 791–809, 2016.

[17] X. Yue, W. S. Schreiner, Y. Kuo, D. Hunt, and C. Rocken, "GNSS radio occultation technique and space weather monitoring," in *Proc. 26th Int. Tech. Meeting Satell. Division Inst. Navigation (ION GNSS+),* 2013, pp. 2508–2522.

[18] Y. M. Bi et al., "An introduction to China FY3 radio occultation mission and its measurement simulation," *Adv. Space Res.,* vol. 49, no. 7, pp. 1191–1197, 2012.

[19] T. Mao et al., "First ionospheric radio-occultation measurements from GNSS occultation sounder on the Chinese Feng-Yun 3C satellite," *IEEE Trans. Geosci. Remote Sens.,* vol. 54, no. 9, pp. 5044–5053, Sep. 2016.

[20] Y. Cai et al., "In-orbit performance of GNOS on-board FY3-C and the enhancements for FY3-D satellite," *Adv. Space Res.,* vol. 60, no. 12, pp. 2812–2821, 2017.

[21] W. Bai et al., "Validation results of maximum S4 index in F-layer derived from GNOS on FY3C satellite," *GPS Solutions,* vol. 23, no. 1, pp. 1–14, 2018.

[22] X. Wang et al., "Improvements of GNOS on-board FY3D," in *Proc. Int. Tech. Meeting Inst. Navigation,* 2016, pp. 829–835.

[23] A. J. Dessler and J. A. Fejer, "Interpretation of Kp index and M-region geomagnetic storms," *Planet. Space Sci.,* vol. 11, no. 5, pp. 505–511, 1963.

[24] J. Bartels, "The standardized index, Ks, and the planetary index, Kp," *IATME Bull.,* vol. 12b, pp. 97–120, 1949.

[25] J. Matzka, C. Stolle, Y. Yamazaki, O. Bronkalla, and A. Morschhauser, "The geomagnetic Kp index and derived indices of geomagnetic activity," *Space Weather,* vol. 19, no. 5, 2021, Art. no. e2020SW002641.

[26] P. R. Straus, P. C. Anderson, and J. E. Danaher, "GPS occultation sensor observations of ionospheric scintillation," *Geophys. Res. Lett.,* vol. 30, no. 8, 2003.

[27] C. Hanuise et al., "From the Sun to the Earth: Impact of the 27–28 May 2003 solar events on the magnetosphere, ionosphere and thermosphere," *Ann. Geophys.,* vol. 24, pp. 129–151, 2006.

[28] L.-C. Tsai, S.-Y. Su, and C.-H. Liu, "Global morphology of ionospheric F-layer scintillations using FS3/COSMIC GPS radio occultation data," *GPS Solutions,* vol. 21, no. 3, pp. 1037–1048, 2017.

[29] Y. Guanglin et al., "Beidou navigation satellite system sounding of the ionosphere from FY-3C GNOS: Preliminary results," *J. Space Sci.,* vol. 39, no. 1, pp. 36–45, 2019.

[30] G. L. Yang et al., "Validation results of NmF2 and hmF2 derived from ionospheric density profiles of GNOS on FY-3C satellite," *Sci. China-Technol. Sci.,* vol. 61, no. 9, pp. 1372–1383, 2018.

[31] L. Hu et al., "Validation of COSMIC ionospheric peak parameters by the measurements of an ionosonde chain in China," *Ann. Geophys.,* vol. 32, no. 10, pp. 1311–1319, 2014.

[32] P. S. Brahmanandam, G. Uma, J. Y. Liu, Y. H. Chu, N. S. Latha Devi, and Y. Kakinami, "Global S4 index variations observed using FORMOSAT-3/COSMIC GPS RO technique during a solar minimum year," *J. Geophys. Res.: Space Phys.,* vol. 117, no. A9, 2012.

[33] W. J. Burke et al., "C/NOFS observations of plasma density and electric field irregularities at post-midnight local times," *Geophys. Res. Lett.,* vol. 36, no. 18, 2009.

Weihua Bai received the Ph.D. degree in space physics from the University of Chinese Academy of Sciences, Beijing, China, in 2008.

He is currently a Professor with National Space Science Center, Chinese Academy of Sciences, Beijing. He is also the director or deputy director in FY3 series GNOS and GNOS-II missions. His current research interests include GNSS radio occultation and GNSS-R remote sensing techniques and their applications.

Yueqiang Sun received the B.S. degree in radio physics from Nanjing University, Nanjing, China, in 1985, and the Ph.D. degree in space physics from the University of Chinese Academy of Sciences, Beijing, China, in 2002.

She devotes to develop GNSS remote sensing and space-borne spatial environment exploration technologies. She has been the Principal Investigator or Vice Principal Investigator of more than 20 missions/projects in manned space flight, FengYun, and National Natural Science Foundation (863) areas. Her research interests include GNSS radio occultation, GNSS-R remote sensing techniques, atmospheric physics, ionospheric physics, magnetic physics, space physics, and so on.

Xiuqing (Scott) Hu received the B.S. degree in atmospheric science from Nanjing University, Nanjing, China, in 1996, the M.S. degree in cartography and geographical information system from Beijing Normal University, Beijing, China, in 2004, and the Ph.D. degree in quantitative remote sensing science from the Institute of Remote Sensing Application, Chinese Academy of Sciences, Beijing, in 2012.

He is currently the Chief Engineer of ground segment system for Fengyun-3 polar orbiting satellites and the team leader of satellites calibration/calibration of National Satellite Meteorological Center, China Meteorological Administration (NSMC/CMA), Beijing. Since 2020, he has also been a Professor of engineering.

Dr. Hu has been selected the Technological Leading Talent of CMA in 2015. He was the previous Chair of GSICS Research Working Group (GRWG).

Guangyuan Tan received the Ph.D. degree in earth and space exploration technology from the University of Chinese Academy of Sciences, Beijing, China, in 2021.

He is currently a Postdoctoral Researcher with the National Space Science Center, Chinese Academy of Sciences, Beijing. His research interests include application and retrieval of ionospheric radio occultation products.

Peng Zhang (Senior Member, IEEE) received the master's degree in atmospheric optics from the Anhui Institute of Optics and Fine Mechanics, Chinese Academy of Sciences, Beijing, China, in 1995, and the Ph.D. degree in atmospheric physics from the Institute of Atmospheric Physics, Chinese Academy of Sciences, in 1998.

Since 2013, he has been the Deputy Director-General of National Satellite Meteorological Center (NSMC/CMA), the Chief Director of FY-3 ground segment since 2013, the Chair of Global Space Inter-Calibration System (GSICS) Executive Panel from 2014 to 2017, and the Chief Director of Chinese TanSat satellite ground segment since 2015. He has the intensive experience in conceiving, developing, and operating FY-3 satellite ground segment. His major research interests include the atmospheric remote sensing, satellite data assimilation, and satellite calibration and validation.

Guanglin Yang received the M.S. degree in atmosphere physics from Peking University, Beijing, China, in 2002.

He is currently a Senior Engineer in ionosphere observation with the National Center for Space Weather, China Meteorological Administration, Beijing. His research interests include GNSS radio occultation, GNSS/MET, and coupling of upper atmosphere and ionosphere.

Jingsong Wang received the M.S. degree from Peking University, Beijing, China in 1994, and the Ph.D. degree from the Center for Space Science and Applied Research, Chinese Academy of Sciences, Beijing, in 1997, both in space physics.

He is currently the Director of the National Satellite Meteorological Center, China Meteorological Administration (NSMC/CMA), Beijing. His research interests include ionospheric weather, space weather monitoring and early warning technology, and satellite meteorology.

Qifei Du received the Ph.D. degree in space physics from the University of Chinese Academy of Sciences, Beijing, China, in 2012.

He was the Principal Investigator of the occultation payloads for Yinghuo satellite and Fengyun-3 satellites. His research focuses on space-borne applications of GNSS signal, including GNSS occultation and GNSS-R remote sensing, GNSS receiver, antenna, and microwave circuits development.

Xianyi Wang received the Ph.D. degree in space physics from the University of Chinese Academy of Sciences, Beijing, China, in 2012.

He is currently a Doctor with National Space Science Center, Chinese Academy of Sciences. His current research interests include digital signal processing of GNSS radio remote sensing, embedded system design, and software system design of satellite receiver.

Congliang Liu received the Ph.D. degree in geodesy and survey engineering from the China University of Mining and Technology, Beijing, China, in 2013.

He is currently a Doctor with National Space Science Center, Chinese Academy of Sciences, Beijing. He currently works on atmosphere and climate monitoring and analysis using radio occultation data. His research focuses on LEO–LEO microwave occultation technique.

Xiangguang Meng received the Ph.D. degree in surveying and mapping engineering from Wuhan University, Wuhan, China, in 2011.

He is currently a Doctor with National Space Science Center, Chinese Academy of Sciences, Beijing, China. His research interests include GNSS precise orbit determination and radio occultation data processing.

Peng Hu received the M.Sc. degree in geodetic surveying from Chang'an University, Xi'an, China, in 2019.

He is currently with National Space Science Center, Chinese Academy of Sciences, Beijing, China. His research interests include GNSS precise orbit determination and the integrated orbit determination of LEO and GNSS satellites.